SCIENTIFIC REPORTS

OPEN

Eigenstress model for electrochemistry of solid surfaces

Hongxin Ma[1], Xilin Xiong[1], Panpan Gao[1], Xi Li[1], Yu Yan[1], Alex A. Volinsky[2] & Yanjing Su[1]

Thermodynamic analysis and molecular dynamics simulations were conducted to systematically study the size-dependent electrochemical response of solids. By combining the generalized Young-Laplace equation with the popular Butler-Volmer formulation, the direct influence of surface stress on solid film electrochemical reactions was isolated. A series of thermodynamic formulas were developed to describe the size-dependent electrochemical properties of the solid surface. These formulas include intrinsic surface elastic parameters, such as surface eigenstress and surface elastic modulus. Metallic films of Au, Pt, Ni, Cu and Fe were studied as examples. The anodic current density of the metal film increased, while the equilibrium potential decreased with increasing solid film thickness.

Surface stress/energy of solids plays a key role in the thermodynamics of solid surfaces, offering the description of macroscopic phenomena, including electrochemical and chemical responses. While the surface-to-volume ratio of nanomaterial is much larger than that of bulk material, this role becomes even more significant in nanomaterials. However, classical electrochemical theory does not completely account for the surface stress/energy of a solid.

Surface stress/energy of solids has been studied over half a century by many researchers[1–3]. When surfaces are created by cutting a crystal along a crystallographic plane, fresh surfaces without relaxation have a much higher surface energy. Atomic simulations[4,5] and experiments[6] have verified that energy minimization of the separated free-standing crystals occurs unavoidably to reduce the surface and the total energy. This relaxation rearranged atoms positions locally to lower the total energy, but may lead to a change in the lattice spacing of a nanometer-sized material, i.e. induce initial strain[7]. Surface relaxation was separated into the surface-normal relaxation and the surface-parallel relaxation[8], which induces deformation parallel to the surface. After relaxation, a tensile (or compressive) surface eigenstress causes a compressive (or tensile) initial strain in the core of the nanomaterial with respect to its bulk lattice. Due to the initial deformation, both the surface energy density and surface stress are size-dependent. Weissmüller *et al.*[8] proved that the surface-parallel and surface-normal deformations are both state variables of the surface free energy.

Dingreville *et al.*[9,10] systematically studied the relationship between the surface energy, surface stress and surface elastic constants within the scheme of continuum mechanics theory. They incorporated the surface free energy into the continuum theory of mechanics demonstrated that the overall elastic behavior of the structural elements (particles, wires, and films) are size-dependent[9]. Although such size-dependency is negligible for conventional structural elements, it becomes significant when at least one of the dimensions of the element shrinks to nanometers. Dingreville *et al.*[11] also analyzed the problem of the interfacial excess energy, excess stress and excess strain of planar interfaces. Their analysis revealed that the surface stress and the surface strain are intrinsic material properties. The in-plane interfacial stiffness tensor, the out-of-plane interfacial compliance tensor, and the coupling tensor, which accounts for the Poisson's effect of the interface, are all independent of the solid geometrical size, and fully describe the elastic behavior of a coherent interface upon deformation.

Interactions between mechanical and electrochemical effects have an influence on the electrode reactions on metal surfaces[12]. Weissmüller *et al.*[8] suggested that in terms of electrochemical experiments under pressure, the electrode potential is pressure-dependent. In some cases, mechanical and electrochemical effects are coupled with each other leading to modified electrochemical reaction rates or corrosion rates of the solid with respect to its stress-free state[13]. From the above discussion, it is reasonable to expect that the size-dependent surface energy/stress of the nanomaterial will lead to size-dependent electrochemical and corrosion properties. Actually, numerical and experimental results show that the electrochemical reaction rate of nanograined materials is size-dependent. As examples, the corrosion resistance properties of 304 stainless steel in NaCl solution[14–17] and iron in alkaline solutions[18] were improved when the material grain size was at the nanometer scale. Despite the

[1]Corrosion and Protection Center, Key Laboratory for Environmental Fracture (MOE), University of Science and Technology Beijing, Beijing 100083, China. [2]Department of Mechanical Engineering, University of South Florida, Tampa, Florida 33620, USA. Correspondence and requests for materials should be addressed to Y.S. (email: yjsu@ustb.edu.cn)
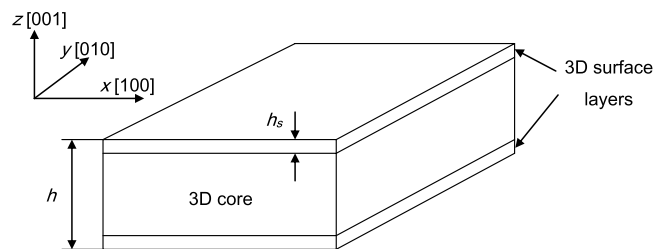
Figure 1. Model of a solid film with (001) surface separated into two 3D surface layers with the thickness h_s coherently adhered to the 3D core with the thickness $h - 2h_s$.

Materials	$\widetilde{\sigma}_s^0$, N/m	$\widetilde{Y}_s$, N/m	σ_s^0, GPa	Y_s, GPa	Y_c, GPa	Z	E_e^{bulk}, V
Pt (001)	2.60	25.73	2.60	109.80	84.08	2	1.20
Au (001)	1.56	14.27	1.56	81.07	66.81	3	1.50
Ni (001)	1.31	21.67	1.31	205.32	183.65	2	−0.25
Cu (001)	1.38	18.20	1.38	125.43	107.23	2	0.35
Fe (001)	2.03	−14.57	2.03	200.92	215.48	2	−0.44

Table 1. Eigenstress $\widetilde{\sigma}_s^0$ and σ_s^0, surface modulus $\widetilde{Y}_s$ and Y_s, bulk modulus Y_c, number of electronic charge Z and the standard electrode potential E_e^{bulk} referred to the SHE. (σ_s^0 and Y_s were calculated based on $h_s = 1$ nm and the surface of (001)).

same chemical composition, the breakdown potential of the sputtered nanocrystalline (grain size approximately 25 nm) 304 type stainless steel film is found to be approximately 850 mV higher than that of the conventional material.[16] The high corrosion resistance of the sputtered film is attributed to the smaller grain size of the film. The similar results were reported by Youssef[19], the estimated corrosion rate of nanocrystalline zinc (56 nm) with random orientation was found to be about 60% lower than that of electrogalvanized steel, 90 and 229 μA/cm^2, respectively. In the work of Mishra[20], the electrochemical and corrosion behavior of nanocrystalline nickel of different grain sizes (8–28 nm) in 1 mol/L H$_2$SO$_4$ electrolyte was compared with that of bulk Ni. The breakdown potential for fine grain sized nanocrystalline nickel was higher than that of coarse-grained polycrystalline nickel. There was a systematically increase in breakdown potential from 1110 mV to 1540 mV (silver-silver chloride reference electrode) with decreasing the grain size to 8 nm. The corrosion rate of freshly exposed nanocrystalline Ni was lower compared to that of bulk Ni, indicating a higher hindrance to anodic dissolution from the nanocrystalline Ni surfaces. On the other hand, an opposite trend was observed experimentally. The corrosion rate of Ti alloy in H$_2$SO$_4$ and HCl solutions was inversely proportional to the square root of the grain size[21]. The corrosion resistance of the Cu$_{90}$Ni$_{10}$ alloy in neutral Cl$^-$-containing solution was reduced when the grain size was at the nanometer scale[22]. Thus, it is necessary to understand and predict the size-dependent electrochemical properties of nanomaterials, which is the subject of the present study.

Electrode reaction rates are commonly modeled using the Butler-Volmer equation[23–26]. The classical form of the Butler-Volmer equation does not incorporate the effect of the surface stress on the reaction rates. Gutman[12] systematically studied the effect of the applied stress on the electrochemical response of bulk materials. In this paper, a stress-dependent chemical potential, obtained using the Gibbs-Duhem equation[27], was used to extend the classical Butler-Volmer equation. The generalized Young-Laplace equation[28] was used to describe the mechanical force balance between the surface and the underlying bulk material. By combining the Young-Laplace equation with the Gibbs-Duhem[27] and the Butler-Volmer[23–26] equations, the dependence of the electrochemical potential on the intrinsic surface elastic parameters, such as the surface eigenstress and surface elastic modulus, was obtained. Intrinsic surface elastic parameters were incorporated to reveal the physical origin of the size-dependent electrochemical corrosion properties, such as the current density of the electrode reactions, along with the equilibrium potentials of solid films.

Results

Intrinsic surface elastic parameters and thickness. A solid film with the (001) surface is modeled as a composite consisting of two 3D surface layers coherently bonded to a 3D core, as shown in Fig. 1. The core and the surface layers are assumed to be mechanically isotropic, linearly elastic, and the surface and core stresses are homogeneous. The orthogonal coordinates x, y, and z were set along the [100], [010], and [001] lattice directions, respectively.

Molecular dynamics (MD) simulations were conducted to extract the 2D intrinsic surface elastic parameters of 2D surface eigenstress, $\widetilde{\sigma}_s^0$, 2D surface biaxial Young's modulus, $\widetilde{Y}_s$, and bulk biaxial Young's modulus Y_c of Pt, Au, Ni, Cu and Fe. The 3D intrinsic surface elastic parameters of 3D surface eigenstress, σ_s^0, and 3D surface biaxial Young's modulus, Y_s, can be got by $\widetilde{\sigma}_s^0 = \sigma_s^0 h_s$ and $\widetilde{Y}_s = (Y_s - Y_c) h_s$, respectively. The intrinsic surface elastic parameters of the (001) surface were summarized in Table 1, with the assumption of the surface layer thickness $h_s = 1$ nm.
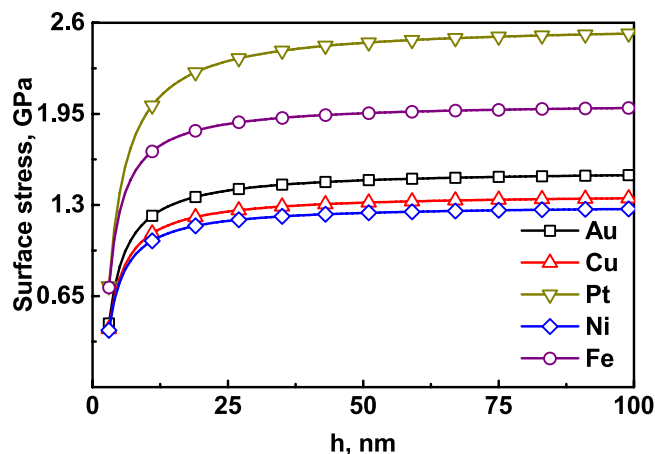
Figure 2. The film surface stress versus the thickness h with $h_s = 1$ nm, based on Eq. (1).

The 3D surface eigenstress and 3D surface biaxial Young's modulus can be determined by above formulas, if one has known the thickness of the surface layer h_s. This is a challenge faced in the interphase surface approach[29]. However, the surface layer thickness is always assumed to be 1 nm in the study of surface thermodynamic properties based on the facts: (1) both theoretical calculations and experimental observations focusing on the similar structure of grain-boundaries have been confirmed and widely accepted that their thickness variations are within the range of 0.4 to 2.0 nm[30–33] and (2) according to the relaxation process of metallic films by MD simulations, the normal-relaxation always occurs in the first five atomic surface layers with the traction-free surfaces, whereas most of the atomic layers in the film maintain undeformed compared with the stress-free bulk crystal[34]. The thickness of the first five atomic surface layers is the double of the lattice constant, which is around 1 nm. Hereafter, we assume that the surface thickness is 1 nm to study the size-dependent electrochemical properties of the solid films.

Size-dependent surface stress of the solid film. At the equilibrium, the biaxial surface stress of the solid film is given by

$$\sigma_s = \sigma_s^0 + Y_s \varepsilon^{ini} = \sigma_s^0 \left[1 - \frac{2h_s Y_s}{2h_s Y_s + (h - 2h_s) Y_c} \right] \tag{1}$$

where σ_s^0 is the biaxial eigenstress in the surfaces, ε^{ini} is the initial strain after parallel relaxation, h_s and h are the thicknesses of the surface layer and the film, and Y_s and Y_c are biaxial Young's modulus of the surface and the core, respectively.

Substituting the data of σ_s^0, Y_s, Y_c and h_s into Eq. (1), we can get the surface stress σ_s of the film versus the film thickness h, as shown in Fig. 2. In the smaller range of the film thickness, the absolute value of the surface stress increases sharply with increasing thickness h. For sufficiently thick films, the surface stress is almost the same as the surface eigenstress of the bulk material.

Size-dependent equilibrium potential of the solid film. The equilibrium potential of the solid film can be described as:

$$\vec{\phi}_e = \phi_e - \frac{2\sigma_s V_m}{3ZF} = \phi_e - \frac{2\sigma_s^0 V_m}{3ZF} \left[1 - \frac{2h_s Y_s}{2h_s Y_s + (h - 2h_s) Y_c} \right] \tag{2}$$

where ϕ_e is the equilibrium potential of the electrode reaction, Z is the number of transferred electrons, F is the Faraday constant, and V_m is the molar volume of the electrode material. When the thickness of the film $h \to \infty$, that is, for the bulk materials, Eq. (2) can be given as:

$$\vec{\phi}_e^{bulk} = \phi_e - \frac{2\sigma_s^0 V_m}{3ZF} \tag{3}$$

Eq. (3) is the general formulas of the equilibrium potential for bulk materials, which take the surface stress into account.

Based on Eq. (2) the equilibrium potential difference between the solid films and the bulk material can be described as the following:

$$\vec{\phi}_e^{film} - \vec{\phi}_e^{bulk} = - \frac{2(\sigma_s - \sigma_s^0) V_m}{3ZF} = \frac{2\sigma_s^0 V_m}{3ZF} \left[\frac{2h_s Y_s}{2h_s Y_s + (h - 2h_s) Y_c} \right] \tag{4}$$
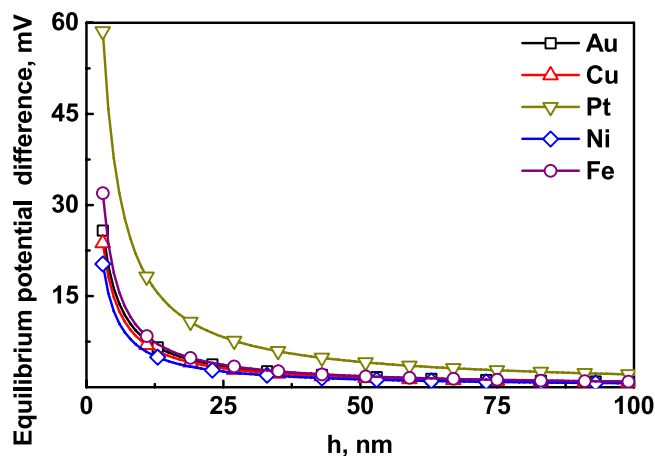
Figure 3. The equilibrium potential difference between the solid films and bulk material versus the film thickness *h* with $h_s = 1$ nm, based on Eq. (4).

Substituting the values in Table 1 into Eq. (4), the equilibrium potential difference between the films and the bulk material versus the film thickness can be received, as shown in Fig. 3. The value of the film equilibrium potential is higher than that of the bulk material. With increasing film thickness *h*, the difference between the solid films and the bulk material decreases to zero.

According to Eq. (4), one can obtain the standard electrode potential of the films E_e^{film} corresponding to the reference electrode of the standard hydrogen electrode (SHE) compared with the bulk material value as a function of the film thickness *h*:

$$E_e^{film} = E_e^{bulk} - \frac{2(\sigma_s - \sigma_s^0)V_m}{3ZF} = E_e^{bulk} + \frac{2\sigma_s^0 V_m}{3ZF}\left[\frac{2h_s Y_s}{2h_s Y_s + (h - 2h_s)Y_c}\right] \tag{5}$$

where E_e^{bulk} is the standard electrode potential corresponding to the reference electrode SHE of the bulk material and listed in Table 1.

Figure 4 shows the standard potential of solid films, referred to the SHE, versus the film thickness *h*. This is similar to the equilibrium potential difference between the film and the bulk material versus the film thickness. The value of the standard potential of the solid film is higher than that of the bulk material, and decreases with increasing thickness of the film.

Size-dependent anodic current density. The surface stress existing in the film only modified the rate of the anodic reactions, i.e. the forward direction of the metal electrode reactions. The current density of the electrochemical reaction of the metal film electrode incorporate the effect of the surface stress can be described as:

$$\vec{j}_f = j_0 \exp\left(\frac{\alpha ZF\eta + 2\sigma_s V_m/3}{RT}\right)$$

$$= j_0 \exp\left(\frac{\alpha ZF\eta}{RT}\right)\exp\left(\frac{2\sigma_s^0 V_m}{3RT}\left[1 - \frac{2h_s Y_s}{2h_s Y_s + (h - 2h_s)Y_c}\right]\right) \tag{6}$$

$$\vec{j}_r = j_r = j_0 \exp\left(-\frac{(1-\alpha)ZF\eta}{RT}\right) \tag{7}$$

$$\vec{J} = \vec{j}_f - \vec{j}_r$$

$$= j_0\left[\exp\left(\frac{\alpha ZF\eta}{RT}\right)\exp\left(\frac{2\sigma_s^0 V_m}{3RT}\left[1 - \frac{2h_s Y_s}{2h_s Y_s + (h - 2h_s)Y_c}\right]\right)\right.$$

$$\left. - \exp\left(-\frac{(1-\alpha)ZF\eta}{RT}\right)\right] \tag{8}$$

where α is the transfer coefficients of the electrochemical reaction, η is the overpotential, *R* is the gas constant, *T* is the absolute temperature, j_0 is the exchange current density when the electrode reaction is in the equilibrium state ($\eta = 0$ and $j_f = j_r$).

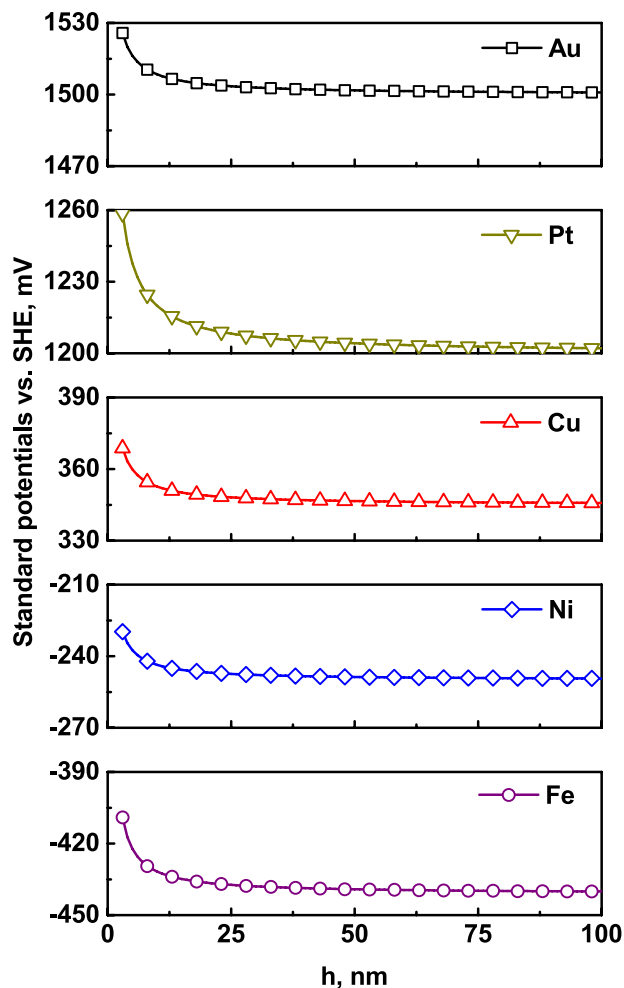When the thickness of the film $h \to \infty$, that is, for the bulk materials, Eq. (8) can be given as:

Figure 4. The standard potential of solid films, referred to the SHE, versus the film thickness h with $h_s = 1$ nm, based on Eq. (5).

$$\overrightarrow{j}^{bulk} = j_0 \left[\exp\left(\frac{\alpha ZF\eta}{RT} \right) \exp\left(\frac{2\sigma_s^0 V_m}{3RT} \right) - \exp\left(-\frac{(1-\alpha)ZF\eta}{RT} \right) \right]$$

(9)

Eq. (9) is the general formulas of the electrochemical reaction rate for bulk materials, which take the surface stress into account.

Based on Eq. (6) one can get the current density ratio of the anodic reactions $\overrightarrow{j}_f^{film} / \overrightarrow{j}_f^{bulk}$ as a function of the film thickness h.

$$\frac{\overrightarrow{j}_f^{film}}{\overrightarrow{j}_f^{bulk}} = \exp\left(\frac{2(\sigma_s - \sigma_s^0)V_m}{3RT} \right) = \exp\left(-\frac{2\sigma_s^0 V_m}{3RT} \frac{2h_s Y_s}{2h_s Y_s + (h - 2h_s)Y_c} \right)$$

(10)

By substituting the data in Table 1, the current density ratio of the anodic reactions between the films and the bulk material versus the film thickness can be received, as shown in Fig. 5. The oxidation current density of the free-standing metal film is lower than that of the bulk material, especially when the value of h is small. The difference will be close to zero when the h value is large enough.

Discussion

The present study focuses on the fundamental elastic properties of a solid surface and considers solid films as typical structures to simplify the theoretical analysis. Usually, there are three common approaches to study the properties of surfaces[29]: the sharp or two-dimensional (2D) surface approach, the diffusive and/or interphase surface approach. Both the diffusive and interphase surface approaches treat surfaces as three-dimensional (3D). In the sharp surface approach, a single dividing interface of zero thickness[35] is used to separate a studied system from its environment and the surface contribution to the thermodynamic properties is defined as the excess over the values that would obtain if the studied system and environment retained their properties constant up to the
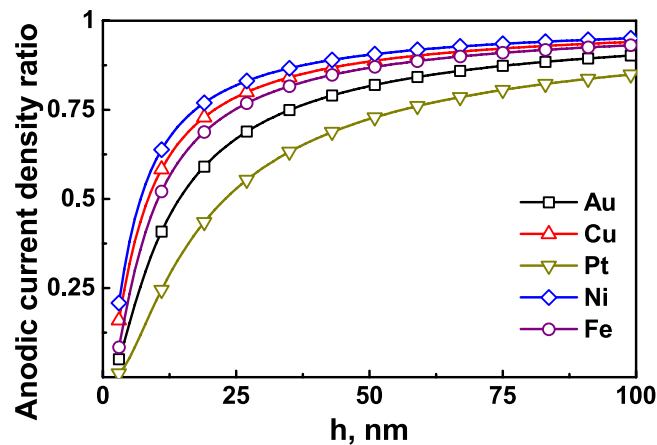
Figure 5. **The current density ratio of the anodic reactions between solid films and bulk materials versus the film thickness** h **with** $h_s = 1$ **nm, based on Eq. (10).**

dividing interface. The diffusive interface is described by a gradient term, e.g., the concentration gradient[36]. The interphase approach treats an interface as a thermodynamic phase, and is usually chosen to be at locations where the properties are no longer varying significantly with the position. The interphase surface has a finite volume (thickness) and may be assigned thermodynamic properties in the normal way. Since the atoms within a very thin layer near surfaces experience a different local environment form that experienced by atoms in bulk, the physical properties and mechanical response of surfaces will be distinct from those of bulk materials. The surface modulus and the interphase interfaces have been generally used in the thermodynamic and mechanical researches of solid surfaces[29,37]. Therefore, the interphase approach is used in the present study to solve the problem of the size dependent electrochemical response of the solid films.

When a solid film is separated from the stress-free bulk substrate, the films will relax reaching equilibrium to meet the energy minimization requirements due to the creation of a new surface. The relaxation process can be separated into normal and parallel relaxation[34]. After normal relaxation, an eigenstress σ_s^0 is created in the surface layer, which is equal to the surface stress σ_s^{bulk} of the bulk material. After parallel relaxation, a stress (or initial strain ε^{ini}) will be generated in the core to balance the surface stress. The surface layers must undergo the same deformation as the core, because the surfaces are coherently adhered to the core, which changes the surface stress from σ_s^0 to σ_s.

If the film state after normal relaxation is taken as the reference configuration, the total potential energy of a solid film is given by:

$$U(\varepsilon) = 2h_s L_0^2 u_s(\varepsilon) + (h - 2h_s)L_0^2 u_c(\varepsilon) \tag{11}$$

where ε denotes the biaxial strain, u_s and u_c are generalized energy densities per unit volume of the surface layer and the core, respectively, and L_0 is the length and width of the film after normal relaxation. Further, h_s and h are the thicknesses of the surface layer and the film, respectively.

The energy density of the surface layer and the core can be written as:

$$u_s(\varepsilon) = u_s^0 + 2\sigma_s^0 \varepsilon + Y_s \varepsilon^2 \tag{12}$$

$$u_c(\varepsilon) = u_c^0 + Y_c \varepsilon^2 \tag{13}$$

where u_s^0 and u_c^0 are the generalized energy densities of the surface layer and the core in the strain-free state, respectively.

Substituting Eqs (12) and (13) into Eq. (11), the total potential energy of a film is given by

$$U(\varepsilon) = 2h_s L_0^2 (u_s^0 + 2\sigma_s^0 \varepsilon + Y_s \varepsilon^2) + (h - 2h_s)L_0^2 (u_c^0 + Y_c \varepsilon^2) \tag{14}$$

At the equilibrium, the energy minimization requires $\partial U(\varepsilon)/\partial \varepsilon \big|_{\varepsilon = \varepsilon^{ini}} = 0$, which yields the generalized Young-Laplace equation[28] to describe the mechanical force balance between the surface layer and the core:

$$2h_s \sigma_s^0 + 2h_s Y_s \varepsilon^{ini} + (h - 2h_s) Y_c \varepsilon^{ini} = 2F_s^{ini} + F_c^{ini} = 0 \tag{15}$$

where $F_c^{ini} = (h - 2h_s)Y_c \varepsilon^{ini}$ and $F_s^{ini} = h_s(\sigma_s^0 + Y_s \varepsilon^{ini})$ denote the core and the surface force per unit length, respectively.

From Eq. (15), the initial strain induced by the surface stress is given by

$$\varepsilon^{ini} = -\frac{2h_s \sigma_s^0}{2h_s Y_s + (h - 2h_s)Y_c} \tag{16}$$

According to the Hooke's law, the biaxial surface stress of the solid film is given by Eq. (1). From Eqs (16) and (1), it is clearly seen that the initial strain and the surface stress of the solid film is size-dependent, i.e. depend on the thickness of the film.

If we introduce 2D surface properties of the 2D surface eigenstress, $\widetilde{\sigma}_s^0$, and 2D surface biaxial modulus, $\widetilde{Y}_s$, Eqs (15), (16) and (1) can be rewritten as
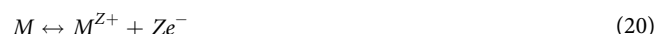
$$2\widetilde{\sigma}_s^0 + 2\widetilde{Y}_s \varepsilon^{ini} + hY_c \varepsilon^{ini} = 0 \tag{17}$$

$$\varepsilon^{ini} = -\frac{2\widetilde{\sigma}_s^0}{2\widetilde{Y}_s + hY_c} \tag{18}$$

$$\widetilde{\sigma}_s = \widetilde{\sigma}_s^0 + \widetilde{Y}_s \varepsilon^{ini} = \widetilde{\sigma}_s^0 \left[1 - \frac{2\widetilde{Y}_s}{2\widetilde{Y}_s + hY_c} \right] \tag{19}$$

where $\widetilde{\sigma}_s^0 = \sigma_s^0 h_s$ and $\widetilde{Y}_s = (Y_s - Y_c)h_s$. Eqs (17) and (18) are the Young-Laplace equation caused by the initial strain and the surface stress in the 2D surface approach[29,35,38].

An elementary electrochemical reaction, developing on the metal electrode surface, can be written as:

$$M \leftrightarrow M^{Z+} + Ze^- \tag{20}$$

where M is the reduced state of a metal, M^{Z+} is the oxidized metal state, e^- is the electron charge, and Z is the number of transferred electrons. Here the anodic direction is considered to be forward and the cathodic direction is reversed. In the anodic direction the metal ions dissolved in the electrolyte from the electrode surface and a current generated from the electrode to the electrolyte.

In general, the electrochemical potential can be expressed as[25,26]

$$\overline{\mu} = \mu + ZF\phi = \mu_0 + RT \ln a + ZF\phi \tag{21}$$

where μ is the chemical potential of the corresponding particles, ϕ is the inner electrical potential of the corresponding phase, a is the activity coefficient, μ_0 is the standard chemical potential when $a = 1$.

In equilibrium, for Eq. (20), the Gibbs free energy $\Delta G = 0$, thus

$$\Delta G = \overline{\mu}_{M^{Z+}} + Z\overline{\mu}_{e^-} - \overline{\mu}_M = \mu_{M^{Z+}} + Z\mu_{e^-} - \mu_M - ZF(\phi_M - \phi_{sol}) = 0 \tag{22}$$

where ϕ_M and ϕ_{sol} are the inner electrical potential of the metal electrode and the electrolyte, respectively. Thus, the equilibrium potential of the electrode reaction can be written as:[25,26]

$$\phi_e = \phi_M - \phi_{sol} = \frac{\mu_{M^{Z+}} + Z\mu_{e^-} - \mu_M}{ZF} \tag{23}$$

Then, for a given overpotential η the net electrochemical reaction rate can be obtained from the well-known Butler-Volmer equation[25,26]:

$$J = j_0 \left[\exp\left(\frac{\alpha ZF\eta}{RT} \right) - \exp\left(-\frac{(1-\alpha)ZF\eta}{RT} \right) \right] \tag{24}$$

where $j_0 = ZFKa = ZFka \exp\left(-\frac{\Delta G^a}{RT} \right)$ is the exchange current density when the electrode reaction is in the equilibrium potential ϕ_e ($\eta = 0$), K is the rate constant, k is the pre-exponential factor, and ΔG^a is the forward or reverse activation energy barrier.

It is well known that for solids there is a linear relationship between the Gibbs free energy and the pressure P. The volume V expanded into exponential series with respect to pressure is mainly described by the zero order term V_0 because of the low compressibility of the solid phase. According to the Gibbs-Duhem equation[27], $\Sigma N_i d\mu_i = -SdT + Vdp$, the linear form of the chemical potential dependence on pressure follows the expression[12]:

$$\Delta\mu = \int_{P_1}^{P_2} V(P)dP = \int_{P_1}^{P_2} V_0 \exp(-\chi P)dP \approx V_0 \Delta P \tag{25}$$

where χ is the compressibility coefficient of the solid ($\chi \approx 10^{-6}$, $\chi P \ll 1$).

If the metal electrode in a system of identical positive ions is simultaneously subjected to the effect of two external factors: mechanical and electrical, the mechano-electrochemical potential can be obtained by combining Eqs (21) and (25)[12]:

$$\ddot{\mu}_M = \mu_{\Delta P=0} + ZF\phi + \Delta PV_m = \mu_0 + RT \ln a + ZF\phi + \Delta PV_m \tag{26}$$

where $\mu_{\Delta P=0}$ is the chemical potential when $\Delta P = 0$ and V_m is the molar volume of the electrode material. The pressure ΔP, applied to the solid metal electrode, has no effect on the electrolyte phase.

Consequently, substituting Eq. (26) into Eq. (22), in the equilibrium state yields:

$$\Delta G = \overline{\mu}_{M^{z+}} + Z\overline{\mu}_{e^-} - \overline{\mu}_M = \mu_{M^{z+}} + Z\mu_{e^-} - \mu_M - ZF(\phi_M - \phi_{sol}) - \Delta P V_m = 0 \qquad (27)$$

Then the equilibrium potential of the electrode reaction under the excess pressure ΔP can be written as[12]:

$$\vec{\phi}_e = \phi_M - \phi_{sol} = \frac{\mu_{M^{z+}} + Z\mu_{e^-} - \mu_M - \Delta P V_m}{ZF} = \phi_e - \frac{\Delta P V_m}{ZF} \qquad (28)$$

Thus, the change of the equilibrium potential due to the applied pressure is

$$\Delta \phi_e = \vec{\phi}_e - \phi_e = -\frac{\Delta P V_m}{ZF} \qquad (29)$$

If the activity coefficient of the intermediate complex does not depend on the potential jump at the electrode-electrolyte boundary, the change of the potential barrier can be regarded as zero when counting the polarization potential $\Delta\phi$. Here, we have introduced the assumption that the potential barrier ΔG^a is independent from the $\Delta\phi$ value[12].

In the event of any mechanical deformation of the electrode, there would be a shift in the chemical/mechano-electrochemical potential of the metal electrode M, based on Eqs (25) and (26), denoted as $\Delta P V_m$. Correspondingly, the free energy of the activation barriers $\Delta\vec{G}_f^a$ in the presence of a stress field is given as:

$$\Delta\vec{G}_f^a = \Delta G_f^a - \Delta P V_m = \Delta\vec{G}_0^a - \alpha ZF\Delta\phi - \Delta P V_m = \Delta\vec{G}_0^a - \alpha ZF\eta - \Delta P V_m \qquad (30)$$

So,

$$\vec{j}_f = ZF\vec{k}\vec{a}\exp\left(-\frac{\Delta\vec{G}_f^a}{RT}\right) = j_0\,\exp\left(\frac{\alpha ZF\eta + \Delta P V_m}{RT}\right) \qquad (31)$$

$$\vec{j}_r = j_r = j_0\,\exp\left(-\frac{(1-\alpha)ZF\eta}{RT}\right) \qquad (32)$$

The current density of the electrode reactions in the presence of the stress are expressed as[12]:

$$\vec{J} = \vec{j}_f - \vec{j}_r = j_0\left[\exp\left(\frac{\alpha ZF\eta + \Delta P V_m}{RT}\right) - \exp\left(-\frac{(1-\alpha)ZF\eta}{RT}\right)\right] \qquad (33)$$

Because applying both the tension and compression stress can increase the chemical potential of the electrode materials, the symbol ΔP refers to the absolute value of the hydrostatic part of the stress tensor.

Surface stress is the key factor for the equilibrium potential and the reaction rate of the electrode reactions, which take place only on the electrode surface. From the biaxial surface stress (σ_s) of the solid film, one can obtain the hydrostatic part of the stress tensor using $\Delta P = 2\sigma_s/3$. By substituting ΔP into Eq. (28), the equilibrium potential of a solid film can be described by Eq. (2).

By substituting ΔP into Eqs (31–33), the current density of the electrochemical reaction of the solid film can be described by Eqs (6–8).

Methods

MD simulations. MD simulations were conducted to study the intrinsic surface elastic parameters of solid films[38]. MD simulations for Au, Pt, Ni, Cu face-centered-cubic crystals and a Fe body-centered-cubic crystal were performed with the LAMMPS code[39]. All crystals were simulated with the embedded-atom method potentials[40,41]. All simulations were conducted in a molecular statics framework and implemented by using the conjugate gradient method.

Bulk biaxial Young's modulus. The simulations were performed on bulk crystals to obtain the bulk biaxial Young's modulus. A representative domain of $8 \times 8 \times 8$ unit cells with periodic boundary conditions (PBCs) in all three directions was adopted to simulate the bulk material. The reference energy U_0 and equilibrium lattice constant in the stress-free bulk crystals were obtained through energy minimization. The bulk biaxial modulus was then determined from simulations of biaxial compressive and tensile tests[38], which were conducted in two steps. (1) All atoms were displaced uniformly in the xy plane according to the uniform biaxial strain with an increment of 0.1%. (2) The plane stress condition in the z direction was identified by adjusting the periodic length along the z direction to achieve the minimum total potential energy configuration. A strain range of -1% to 1% was adopted, corresponding to the initial strains in thin films, discussed in the next section.

Since the unloading data overlap completely with the loading data indicates that the bulk crystals deform elastically within the applied strain range. Furthermore, under the traction-free conditions along the z direction, the strain energy density ($U_c - U_0$) versus the applied biaxial strain ε_c was well fitted using a quadratic function ($U_c - U_0$) = $Y_c\varepsilon_c^2$, as shown by the solid lines in Fig. 6, where Y_c is the bulk biaxial Young's modulus was calculated from the second derivatives of the strain energy with respect to the applied strain. These bulk biaxial Young's modulus Y_c were listed in Table 1.
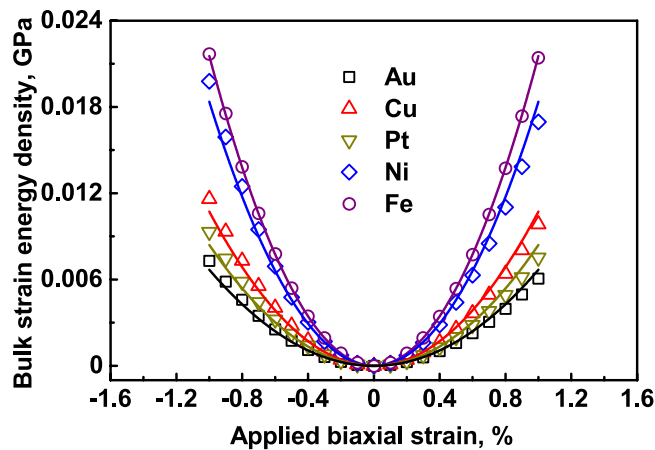
Figure 6. Strain energy per unit volume as a function of the biaxial strain, where solid lines are the fitting curves using $(U_c - U_0) = Y_c \, \varepsilon_c^2$ and biaxial strain loading is applied along the [100] and [010] directions, while the [001] direction is traction free.
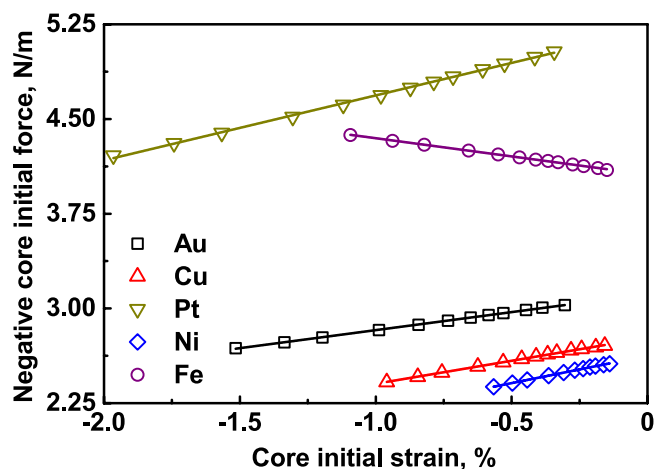

Figure 7. Negative core initial force plotted versus initial strain, for the (001) solid films, where solid lines are fitting curves using Eq. (17).

Surface eigenstress and surface biaxial Young's modulus. For solid film simulations, a film was created by placing atoms with the stress-free bulk lattice constant. To simulate a representative element of an infinitely large film, PBCs were applied only in the x and y directions with the free (001) surfaces in the z direction. Film thickness h was determined from the volume[38] of the simulated representative film in its undistorted configuration with the film length and width equal L_0. The undistorted volume multiplied by the density of the bulk crystal represented the total mass of the atoms in the film. The film thickness ranged from 2 to 100 nm and the representative element had a size of 8×8 unit cells in the x and y directions. The relaxation of the solid film towards the minimal energy state was separated into two steps, i.e., normal and parallel relaxations[38]. In normal relaxation, atoms were allowed to move in the z direction to minimize the total energy with the prescribed representative film length L_0 in both x and y directions. After normal relaxation, parallel relaxation was conducted, in which atoms were allowed to move in all three directions. For a given number of unit cells in the representative film, the total film energy depends on the representative film length L. When the parallel relaxation reaches the final equilibrium state, the energy is minimized and the representative film length has its initial value L^{ini}. Once the initial representative film length was determined, the initial strain ε^{ini} of the film was calculated as $\varepsilon^{ini} = \ln(L^{ini}/L_0)$.

Then the fitting lines $-F_c^{ini} = -hY_c \varepsilon^{ini}$ plotted versus ε^{ini} yield the $2\widetilde{Y}_s$ slope and the $2\widetilde{\sigma}_s^0$ intersection, meaning that the 2D surface biaxial Young's modulus $\widetilde{Y}_s$ and eigenstress $\widetilde{\sigma}_s^0$ can be determined. Figure 7 shows the negative initial core force $(-F_c^{ini})$ as a function of the core initial strain (ε^{ini}), where the solid lines are fitting results based on equation $-hY_c \varepsilon^{ini} = 2\widetilde{\sigma}_s^0 + 2\widetilde{Y}_s \varepsilon^{ini}$.

The intrinsic surface elastic parameters of the eigenstress $(\widetilde{\sigma}_s^0)$ and the biaxial Young's modulus $(\widetilde{Y}_s)$, and the bulk biaxial Young's modulus (Y_c) of Pt, Au, Ni, Cu and Fe are summarized in Table 1.

Theoretical analysis. Thermodynamic expressions for the size-dependent surface stress, equilibrium potential, and the anodic current density in the solid films were developed based on the MD simulations. Furthermore, an extended form of the popular Butler-Volmer equation was used for modeling electrode reaction rates. The shift in the chemical potential used in the Butler-Volmer equation was determined using the Gibbs-Duhem equation. The theoretical analysis and methodology developed in the present work shows that the surface stress, equilibrium potential, and the oxidation current density in the solid films were size-dependent. The anodic current density of a metal film electrode reaction increased and the equilibrium potential decreased with increasing solid film thickness due to the surface energy/stress of the solid films decreasing with respect to bulk materials.

References

1. Shuttleworth, R. The Surface Tension of Solids. *Proc. Phys. Soc. A* **63,** 444 (1950).
2. Nicolson, M. M. Surface tension in ionic crystals. *Proc. R. Soc. London, Ser. A* **228,** 490–510 (1955).
3. Orowan, E. Surface energy and surface tension in solids and liquids. *Proc. R. Soc. London, Ser. A* **316,** 473–491 (1970).
4. Diao, J., Gall, K., Dunn, M. L. & Zimmerman, J. A. Atomistic simulations of the yielding of gold nanowires. *Acta Mater.* **54,** 643–653 (2006).
5. Liang, H., Upmanyu, M. & Huang, H. Size-dependent elasticity of nanowires: Nonlinear effects. *Phys. Rev. B* **71,** 241403 (2005).
6. Huang, W. J. *et al.* Coordination-dependent surface atomic contraction in nanocrystals revealed by coherent diffraction. *Nat. Mater.* **7,** 308–313 (2008).
7. Zhang, T. Y., Luo, M. & Chan, W. K. Size-dependent surface stress, surface stiffness, and Young's modulus of hexagonal prism [111] β-SiC nanowires. *J. Appl. Phys.* **103,** 104308 (2008).
8. Weissmüller, J. & Kramer, D. Balance of force at curved solid metal-liquid electrolyte interfaces. *Langmuir* **21,** 4592–4603 (2005).
9. Dingreville, R., Qu, J. & Mohammed, C. Surface free energy and its effect on the elastic behavior of nano-sized particles, wires and films. *J. Mech. Phys. Solids* **53,** 1827–1854 (2005).
10. Dingreville, R. & Qu, J. A semi-analytical method to compute surface elastic properties. *Acta Mater.* **55,** 141–147 (2007).
11. Dingreville, R. & Qu, J. Interfacial excess energy, excess stress and excess strain in elastic solids: Planar interfaces. *J. Mech. Phys. Solids* **56,** 1944–1954 (2008).
12. Gutman, E. M. *Mechanochemistry of materials.* (Cambridge Int Science Publishing, 1998).
13. Sarkar, S. & Aquino, W. Changes in electrodic reaction rates due to elastic stress and stress-induced surface patterns. *Electrochim. Acta* **111,** 814–822 (2013).
14. Wang, X. Y. & Li, D. Y. Mechanical, electrochemical and tribological properties of nano-crystalline surface of 304 stainless steel. *Wear* **255,** 836–845 (2003).
15. Wang, X. Y. & Li, D. Y. Mechanical and electrochemical behavior of nanocrystalline surface of 304 stainless steel. *Electrochim. Acta* **47,** 3939–3947 (2002).
16. Inturi, R. & Szklarska-Smialowska, Z. Localized corrosion of nanocrystalline 304 type stainless steel films. *Corrosion* **48,** 398–403 (1992).
17. Afshari, V. & Dehghanian, C. Effects of grain size on the electrochemical corrosion behaviour of electrodeposited nanocrystalline Fe coatings in alkaline solution. *Corros. Sci.* **51,** 1844–1849 (2009).
18. Afshari, V. & Dehghanian, C. The effect of pure iron in a nanocrystalline grain size on the corrosion inhibitor behavior of sodium benzoate in near-neutral aqueous solution. *Mater. Chem. Phys.* **124,** 466–471 (2010).
19. Youssef, K. M. S., Koch, C. C. & Fedkiw, P. S. Improved corrosion behavior of nanocrystalline zinc produced by pulse-current electrodeposition. *Corros. Sci.* **46,** 51–64 (2004).
20. Mishra, R. & Balasubramaniam, R. Effect of nanocrystalline grain size on the electrochemical and corrosion behavior of nickel. *Corros. Sci.* **46,** 3019–3029 (2004).
21. Barbucci, A., Farne, G., Matteazzi, P., Riccieri, R. & Cerisola, G. Corrosion behaviour of nanocrystalline Cu90Ni10 alloy in neutral solution containing chlorides. *Corros. Sci.* **41,** 463–475 (1998).
22. Bockris, J., Reddy, A. & Gamboa-Aldeco, M. (Springer, New York, 2001).
23. Bard, A. J. & Faulkner, L. R. *Electrochemical methods: fundamentals and applications*, 2nd ed., Vol. 2 (Wiley New York, 2000).
24. Dill, K. A. & Bromberg, S. *Molecular Driving Forces: Statistical Thermodynamics in Chemistry and Biology*, 1st ed., Garland Science, 2002.
25. Bockris, J. M. & Reddy, A. K. *Modern electrochemistry: an introduction to an interdisciplinary area.*, (Plenum Press, 1970).
26. Koryta, J., Dvorak, J. & Bond, A. M. (John Wiley & Sons Ltd, New York, 1987).
27. McFadden, G. B. & Wheeler, A. On the Gibbs adsorption equation and diffuse interface models. *Proc. R. Soc. London, Ser. A* **458,** 1129–1149 (2002).
28. Chen, T., Chiu, M. S. & Weng, C. N. Derivation of the generalized Young-Laplace equation of curved interfaces in nanoscaled solids. *J. Appl. Phys.* **100,** 074308 (2006).
29. Zhang, T. Y. & Ren, H. Solute Concentrations and Strains in Nanoparticles. *Journal of Thermal Stresses* **36,** 626–645 (2013).
30. Yeheskel, O., Chaim, R., Shen, Z. & Nygren, M. Elastic moduli of grain boundaries in nanocrystalline MgO ceramics. *J. Mater. Res.* **20,** 719–725 (2005).
31. Marquardt, H. *et al.* Elastic properties of MgO nanocrystals and grain boundaries at high pressures by Brillouin scattering. *Phys. Rev. B* **84,** 064131 (2011).
32. Zhu, L. & Zheng, X. Influence of interface energy and grain boundary on the elastic modulus of nanocrystalline materials. *Acta Mechanica* **213,** 223–234 (2010).
33. Chaim, R. Percolative composite model for prediction of the properties of nanocrystalline materials. *J. Mater. Res.* **12,** 1828–1836 (1997).
34. Zhang, T. Y., Ren, H., Wang, Z. J. & Sun, S. Surface eigen-displacement and surface Poisson's ratios of solids. *Acta Mater.* **59,** 4437–4447 (2011).
35. Gibbs, J. (Longmans (New-York), Green (New-York), 1928).
36. Cahn, J. W. On spinodal decomposition. *Acta Metall.* **9,** 795–801 (1961).
37. Wang, G. F. & Feng, X. Q. Effects of surface elasticity and residual surface tension on the natural frequency of microbeams. *Appl. Phys. Lett.* **90,** 231904 (2007).
38. Zhang, T. Y., Wang, Z. J. & Chan, W. K. Eigenstress model for surface stress of solids. *Phys. Rev. B* **81,** 195427 (2010).
39. Plimpton, S. Fast Parallel Algorithms for Short-Range Molecular Dynamics. *J. Comput. Phys.* **117,** 1–19 (1995).
40. Foiles, S. M., Baskes, M. I. & Daw, M. S. Embedded-atom-method functions for the fcc metals Cu, Ag, Au, Ni, Pd, Pt, and their alloys. *Phys. Rev. B* **33,** 7983–7991 (1986).
41. Mendelev, M. I. *et al.* Development of new interatomic potentials appropriate for crystalline and liquid iron. *Philos. Mag.* **83,** 3977–3994 (2003).

Author Contributions

Y.S. conceived the study. H.M., X.X., P.G. and Y.S. conducted the study. H.M. processed the data and constructed the figures. Y.S., H.M. and P.G. wrote the manuscript, X.L., Y.Y. and A.A.V. contributed to the review and editing of the manuscript.

Additional Information

Competing financial interests: The authors declare no competing financial interests.

How to cite this article: Ma, H. *et al.* Eigenstress model for electrochemistry of solid surfaces. *Sci. Rep.* **6**, 26897; doi: 10.1038/srep26897 (2016).